and neglected $(\mathrm{Im}\alpha_s/\alpha_s)^2$ since it is of order 10^{-2} in reality. See Sec. IV.

[21]Except for the zeros such as $\alpha_s - \alpha_u$ = fixed.

[22]R. Odorico, Phys. Lett. 38B, 411 (1972).

[23]For example, the condition $\alpha_s + \alpha_t + \alpha_u = 1$ is well satisfied with the Y_1^* trajectory, but not with Y_0^* $[\bar{\alpha}_{Y_0^*}(s) + \alpha_\rho(t) + \bar{\alpha}_{Y_0^*}(u) \sim 0.4$ where $\bar{\alpha} \equiv \alpha - \frac{1}{2}]$.

[24]Particle Data Group, Phys. Lett. 39B, 1 (1972).

[25]C. Lovelace, Phys. Lett. 28B, 264 (1968).

[26]C. Schmid, in *Phenomenology in Particle Physics, 1971,* edited by C. B. Chiu, G. C. Fox, and A. J. G. Hey (Caltech, Pasadena, Calif., 1971).

[27]R. J. N. Phillips, lectures at the 1972 CERN School of Physics (unpublished).

PHYSICAL REVIEW D VOLUME 8, NUMBER 5 1 SEPTEMBER 1973

Matrix Padé Approximants for the $^1S_0$ and $^3P_0$ Partial Waves in Nucleon-Nucleon Scattering*

J. Fleischer, J. L. Gammel, and M. T. Menzel

Department of Physics, Los Alamos Scientific Laboratory, University of California, Los Alamos, New Mexico 87544

(Received 23 April 1973)

In order to correct the threshold behavior of scalar Padé approximants in NN scattering, "matrix Padé approximants," which take into account the various positive- and negative-energy states, have been considered by several authors. In a recent paper by Bessis, Turchetti, and Wortman, truncated matrices based on an incomplete set of basis states were used and a qualitative description of the energy dependence of the $^3P_0$ phase shift was obtained. In this work it is shown that this result is not obtained when a complete set of basis states is used. The main effect of matrix Padé approximants using a complete set of basis states is to introduce an additional attraction at higher energies. Our analysis of the fourth-order graphs is done in a way which allows the external momenta to be completely off shell so that the irreducible graphs can be used as kernels in the Bethe-Salpeter equation. This will make possible the calculation of several higher-order graphs by iterating the Bethe-Salpeter equation.

I. INTRODUCTION

Nucleon-nucleon scattering, in particular for partial waves $L \geq 1$ (L being the orbital angular momentum) and low energies, is an appropriate case in which to study whether Padé approximants can be successfully applied to the summation of the perturbation series of a strong-interaction Lagrangian. The reason is that the phase shifts do not exhibit a resonance behavior and that therefore the perturbation theory can be assumed not to be too drastically divergent. Earlier calculations[1] show that the Born term alone describes higher partial waves reasonably well, and one can therefore hope that P waves and higher waves can be described by a manageable higher-order calculation.

In this paper we investigate a fourth-order calculation in the Yukawa model with the interaction Lagrangian

$$\mathcal{L}_{\mathrm{int}} = -ig\bar{\psi}\gamma_5\vec{\tau}\cdot\vec{\phi}\psi \tag{1}$$

of pseudoscalar pion-nucleon interaction.

A deficiency of low-order Padé approximants has been that the Born term in many partial waves $[^1S_0, {}^3P_2, {}^3D_3, \ldots$ (see Ref. 2)] has an anomalous threshold behavior. For the $^1S_0$ wave, e.g., the Born term behaves like a P wave at threshold ($\sim p^3$, p being the modulus of the c.m. momentum). As the fourth-order term has a normal threshold behavior ($\sim p$), the [1/1] Padé approximant behaves like a D wave, and also sharp resonances at low energies occur.[3] This deficiency has been cured by Bessis, Turchetti, and Wortman[4] and before that by Barlow and Bergère,[5] following Bessis's suggestion. These authors considered "matrix Padé approximants" by taking matrix elements between the various positive- and negative-energy states. The elements of these matrices have in general a normal threshold behavior, and therefore forming Padé approximants in this space does in fact correct the threshold behavior. Furthermore it is hoped that the use of these matrix Padé approximants will improve the convergence because the whole matrices contain more information than just the physical element.

The authors of Ref. 4 did not perform a calculation of the complete matrices. They used the same set of basis states used by Barlow and Bergère, which, although sufficient at threshold,

where it was applied by Barlow and Bergère, is incomplete at positive energies. Their conclusions for higher energies (up to $E_{\text{lab}} \sim 400$ MeV) drawn from these "truncated" Padé approximants seem to be not correct according to our calculation. In particular the decrease of the $^3P_0$ phase shift at higher energy which they obtained from a [1/1] matrix Padé approximant does not occur once one uses a complete set of basis states.

Thus it seems to us that the matrix Padé approximants do not contain as much physics as the authors of Ref. 4 imply, though we still consider them a very useful tool in the summation of the perturbation series of a strong-interaction field theory. We consider it absolutely necessary, however, to attack higher-order calculations, and as a preparation for that we allow the external momenta of the fourth-order graphs to be completely off shell in order to obtain higher-order graphs by iterating the Bethe-Salpeter equation. Apart from this, these kernels will also be useful in a Bethe-Salpeter calculation itself.

As the Dirac algebra becomes quite involved for the complete spin matrices, we have at present performed a calculation only for the $J=0$ states $^1S_0$ and $^3P_0$. The calculation of higher partial waves is feasible, however, and a description of a REDUCE code which does these calculations has been given in Ref. 6. The formula-manipulating language REDUCE[7] has been of great advantage in the calculation of the $J=0$ partial waves in this paper as well.

II. CALCULATION OF THE [1/1] MATRIX PADÉ APPROXIMANT FROM YUKAWA THEORY

We do not wish to repeat all of the contents of Refs. 6, 8, and 9. However, at least some details may be useful for purposes of self-containment.

Since nucleons have positive and negative energy, as they have spin up and down, there is an exact analogy with the spin states of two nucleons. We speak of "energy spin." The states are

$$\text{energy-spin triplet} \begin{cases} ++ & \equiv + , \\ \dfrac{+-\oplus -+}{\sqrt{2}} & \equiv e , \\ -- & \equiv - , \end{cases} \qquad \text{energy-spin singlet} \quad \frac{+-\ominus -+}{2} \equiv o . \tag{2}$$

$\oplus$ and $\ominus$ are arithmetic operations, and the symbols e and o refer to even and odd, respectively.

The four-momenta on the external legs of a graph are labeled as shown in Fig. 1. Partial-wave amplitudes (off shell) will be denoted by $\phi(p_0, p, \alpha, q_0, q, \beta)$, where p and q are the magnitudes of the three-vectors $\vec{p}$ and $\vec{q}$ and the labels

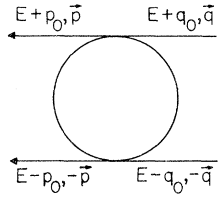

FIG. 1. Labeling of the external momenta of the fourth-order Feynman graphs.

α and β indicate states of definite J (total angular momentum), L (orbital angular momentum), parity, spin, and energy-spin. These states are classified as simultaneous eigenstates of the parity operator P (negative- and positive-energy states have opposite parity) and the exchange operator P_H.[8] The latter operator is a generalization of the Heisenberg exchange operator (P_H also operates in energy-spin space) of nonrelativistic quantum mechanics and essentially embodies the Pauli principle. It also contains the parity operator with respect to the relative energy p_0.

In this paper we are concerned with the $J=0$ partial waves $^1S_0$ and $^3P_0$. According to the above classification,[8] the following states couple in these two cases, respectively:

$$^1S_0^+ , {}^1S_0^- , {}^3P_0^e , {}^3P_0^o$$

and

$$^3P_0^+ , {}^3P_0^- , {}^1S_0^e , {}^3S_0^o ,$$

where the upper right-hand index labels the energy state. Thus the off-shell amplitudes are 4×4 matrices (α and β ranging 1 through 4, representing the above states).

On shell, however, these matrices have zero elements for $\beta=4$ and $\alpha=1,2,3$, and also $\alpha=4$ and $\beta=1,2,3$, because the $^3P_0^o$ and $^1S_0^o$ states are odd in the relative energy p_0, which is zero on shell. Thus the 4×4 matrices degenerate on shell into a 3×3 and a 1×1 matrix, and in forming Padé approximants we only have to take into account the 3×3 part.

As in Ref. 9, we define the tangent matrix

$$(\tan\delta)_{\alpha\beta} = \frac{E}{2\hat{p}}\,\phi(0,\hat{p},\alpha,0,\hat{p},\beta) \quad (\hat{p}^2 = E^2 + m^2) , \tag{3}$$

the $(1,1)$ element of which gives us the physical phase shift. The Yukawa theory results in an expansion

$$(\tan\delta)_{\alpha\beta} = (K_1)_{\alpha\beta}(g^2/4\pi) + (K_2)_{\alpha\beta}(g^2/4\pi)^2 + \cdots , \tag{4}$$

where K_1 and K_2 are matrices. All graphs of order

g^2 and g^4 resulting from the Yukawa coupling are shown in Fig. 2. The calculation of these graphs is described in Appendix A. The usual Feynman rules and renormalization theory apply. The physical or (1, 1) element of the nucleon self-mass contribution vanishes because the external momenta are on shell. The other elements are not on the physical energy shell and do not vanish. The direct box graph is calculated by iterating the Bethe-Salpeter equation as described in Refs. 9 and 10.

The [1/1] matrix Padé approximant is

$$(\tan\delta)_{\alpha\beta}=\left(\frac{g^2}{4\pi}\right)\left(K_1\cdot\frac{1}{K_1-(g^2/4\pi)K_2}\cdot K_1\right)_{\alpha\beta}. \quad (5)$$

The dots stand for matrix multiplication, and the inverse is a matrix inverse. Properties of matrix Padé approximants are discussed in Ref. 11.

III. NUMERICAL RESULTS OF THE MATRIX PADÉ CALCULATION

Our results for the $^1S_0$ and $^3P_0$ phase shifts do not confirm the calculations of Ref. 4. Their most important result seems to us the qualitative agreement of the $^3P_0$ phase shift with experiment. From potential theory one knows that the decrease of the $^3P_0$ phase shift at high energy is due to an $L\cdot S$ coupling, and it was hoped that this would be simulated by a fourth-order matrix-Padé calculation in the Yukawa model. This is, however, not true according to our calculation.

The result for the $^3P_0$ wave in Ref. 4 is mainly due to the way the set of basis states was truncated. In the first place, any truncation is a bad approximation, because in this case in the calculation of a P state one is leaving out an S-state contribution ($^1S_0{}^e$; compare the above labeling of the matrix). Secondly, the authors of Ref. 4 used as definition for the negative-energy states

$$\gamma_5 u(\vec{p}), \quad (6)$$

which are not orthogonal to the positive-energy states. Doing the partial-wave projection we follow the procedure outlined in Refs. 6 and 8, and our definition of the negative energy states is accordingly

$$\gamma_5 u(-\vec{p}). \quad (7)$$

For $J=0$ the relation between the states of Ref. 4 and ours is given by

$$|\alpha\rangle^B = T|\beta\rangle, \quad (8)$$

where the upper left-hand index B refers to the states used in Ref. 4 and

$$T=T^{(1)}\cdot T^{(2)},$$

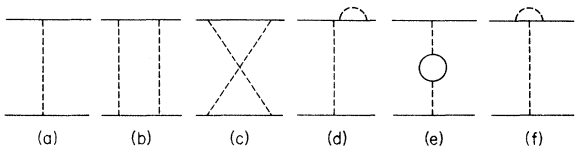

FIG. 2. Feynman graphs of order g^2 and g^4 in the Yukawa model.

with

$$T^{(1)}=\frac{1+\rho_z^{(1)}}{2}+\frac{1-x^2}{1+x^2}\frac{1-\rho_z^{(1)}}{2}+\frac{2\vec{\sigma}^{(1)}\cdot\vec{x}}{1+x^2}\frac{\rho_x^{(1)}+i\rho_y^{(1)}}{2}, \quad (9)$$

$$T^{(2)}=\frac{1+\rho_z^{(2)}}{2}+\frac{1-x^2}{1+x^2}\frac{1-\rho_z^{(2)}}{2}-\frac{2\vec{\sigma}^{(2)}\cdot\vec{x}}{1+x^2}\frac{\rho_x^{(2)}+i\rho_y^{(2)}}{2},$$

$$\vec{x}=\frac{\vec{p}}{E(p)+m}, \quad x=|\vec{x}|.$$

Here σ and ρ are Pauli matrices acting in spin and energy-spin space, respectively.[10] We find

$$\begin{aligned} T\cdot{}^1S_0{}^+ &= {}^1S_0{}^+, \\ T\cdot{}^1S_0{}^- &= \left(\frac{1-x^2}{1+x^2}\right)^2 {}^1S_0{}^- + \left(\frac{2x}{1+x^2}\right)^2 {}^1S_0{}^+ \\ &\quad + \frac{2x}{1+x^2}\frac{1-x^2}{1+x^2}\sqrt{2}\,{}^3P_0{}^e, \end{aligned} \quad (10)$$

and similarly

$$\begin{aligned} T\cdot{}^3P_0{}^+ &= {}^3P_0{}^+, \\ T\cdot{}^3P_0{}^- &= \left(\frac{1-x^2}{1+x^2}\right)^2 {}^3P_0{}^- + \left(\frac{2x}{1+x^2}\right)^2 {}^3P_0{}^+ \\ &\quad + \frac{2x}{1+x^2}\frac{1-x^2}{1+x^2}\sqrt{2}\,{}^1S_0{}^e. \end{aligned} \quad (11)$$

Though the authors of Ref. 4 have not said what their complete set of states would be, assuming relation (8) for $\alpha=3$ and 4 as well the matrices in both cases are related by a nonunitary linear transformation. For matrix Padé approximants we now have the following convariance property:

$$T^\dagger[M/N]_{K_i}T=[M/N]_{T^\dagger K_i T}; \quad (12)$$

that is, we obtain the same result if we form at first the Padé approximant with the original coefficients K_i and then apply the transformation T or transform at first the coefficients K_i and then form a matrix Padé approximant. This is valid for any linear transformation T.[11]

As the transformation T leaves the (1, 1) element invariant [see Eqs. (10) and (11)] — and only this is of physical interest — it is clear that the choice of negative-energy states does not make any difference in the calculation of the physical phase shift from matrix Padé approximants. It does, however, make an important difference when the matrix is

truncated. One could obtain many different results by truncating different sets of basis states. In fact, our calculation shows that with our basis, the negative-energy states being defined by (7), there is practically no decrease at high energy in the $^3P_0$ phase shift (which comes out to be very similar to the scalar approximant) when one calculates a "truncated" Padé approximant by leaving out the third state.

Taking into account the complete basis, one obtains a phase shift which has even more attraction in it, rising up to about 60° without any decrease at high energy — in complete disagreement with Ref. 4. It should be noted, however, that up to about 50 MeV our results are in good agreement with the results of Ref. 4 (see Fig. 3[12]).

For the $^1S_0$ phase shift our results do not differ essentially from the ones of Ref. 4. The sign of the three-momentum in the definition of the negative-energy states is obviously of no importance in the definition of an S wave, and in addition the truncation has no important consequences since one is leaving out a P-wave contribution ($^3P_0{}^e$) in the calculation of an S wave. Thus our calculation yields only some slight additional attraction (Fig. 4).

In Figs. 3 and 4 we have also plotted the results for the [1/1] scalar Padé approximant. Comparison of the matrix Padé approximant with the latter one indicates that the off-shell effects in spin space (with the four-momenta on shell) introduce an additional attraction. This is similar to off-shell effects in momentum space, observed in calculations based on the Blankenbecler-Sugar equation.[13] Apart from the improvement of the threshold behavior of the scalar Padé approximants, we consider this the main significance of the matrix Padé approximants, and this property may in fact become of great importance in a higher-order perturbation theory, where strong repulsive forces will come in through $\pi\pi$ interaction terms in the Lagrangian, e.g., $\lambda\phi^4$, which has not been considered in the present work.

We have checked our graph calculations against those of Ref. 4 at $E_{\text{lab}} = 50$ MeV. Using the connection deduced from Eqs. (8)–(11) between our matrix elements and those of Ref. 4, we obtain complete agreement Numerical results for the graphs in Fig. 2 are given in Tables I and II.

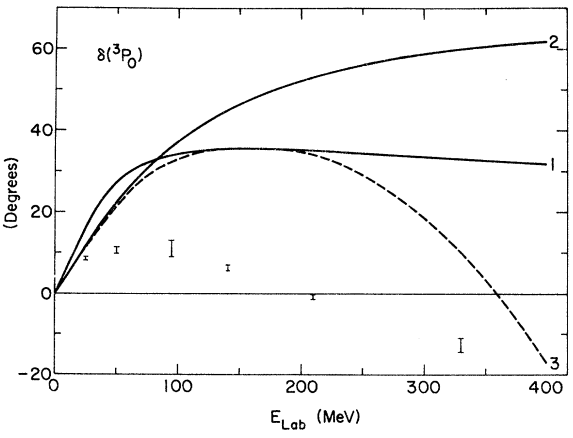

FIG. 3. Results for the $^3P_0$ phase shift $\delta(g^2/4\pi = 14.7)$. Curve 1: scalar Padé approximant. Curve 2: matrix Padé approximant with complete basis set. Curve 3: matrix Padé approximant with truncated basis set taken from Ref. 4; the experimental data are taken from Ref. 12.

ACKNOWLEDGMENTS

One of us (J. F.) wants to thank Professor A. C. Hearn for his continuous assistance in the use of REDUCE. A checking of the renormalization of the nucleon self-mass by Dr. W. Weihofen has been very helpful. Discussions with Dr. W. Wortman and a communication about numerical results for the fourth-order Feynman graphs are gratefully acknowledged.

APPENDIX A

In this appendix we give some details of the calculation of Feynman graphs (off shell) and second-order renormalization. The results are finally given in terms of Feynman integrals rather than dispersion relations. This procedure seems to be particularly adequate for higher-order calculations, for which the present work serves partially as preparation.

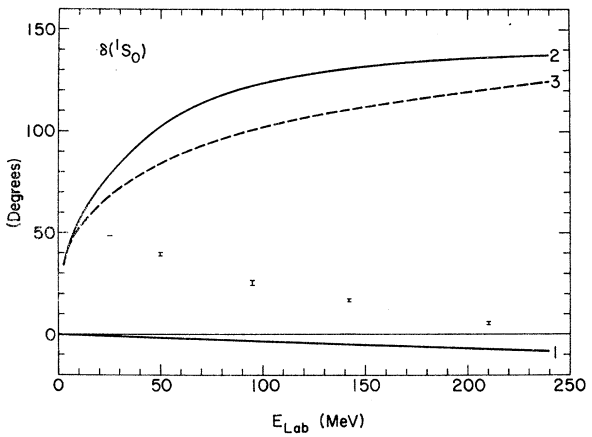

FIG. 4. Same as Fig. 3 for the $^1S_0$ phase shift.

TABLE I. Numerical results for the Feynman graphs of Fig. 2 for the $^1S_0$ partial wave at 50 and 200 MeV. The matrices are symmetric and we therefore have to present only six elements. We have put $g^2/4\pi = 1$.

	Fig.	(1, 1)	(1, 2)	(1, 3) [a]	(2, 2) [a]	(2, 3) [a]	(3, 3) [a]
50 MeV	2(a)	-2.57×10^{-2}	-2.74×10^{0}	-2.23×10^{-1}	-2.57×10^{-2}	2.23×10^{-1}	8.30×10^{-1}
	2(b)	7.94×10^{-3}	8.27×10^{-2}	6.87×10^{-3}	1.99×10^{0}	1.56×10^{-2}	-1.42×10^{-2}
	2(c)	1.21×10^{-2}	-1.02×10^{-1}	6.03×10^{-3}	3.40×10^{0}	1.69×10^{-1}	-7.88×10^{-3}
	2(d)	0	9.20×10^{-1}	3.81×10^{-2}	0	-3.81×10^{-2}	-2.60×10^{-1}
	2(e)	-1.14×10^{-4}	-8.65×10^{-3}	-9.84×10^{-4}	-1.14×10^{-4}	9.84×10^{-4}	2.43×10^{-4}
	2(f)	5.47×10^{-5}	-7.15×10^{-1}	-2.92×10^{-2}	2.02×10^{-2}	-5.78×10^{-2}	1.94×10^{-1}
200 MeV	2(a)	-6.57×10^{-2}	-2.38×10^{0}	-2.84×10^{-1}	-6.57×10^{-2}	2.84×10^{-1}	1.21×10^{0}
	2(b)	1.45×10^{-2}	7.44×10^{-2}	9.36×10^{-3}	-9.25×10^{-2}	-2.09×10^{-1}	-6.99×10^{-2}
	2(c)	1.54×10^{-2}	-1.65×10^{-1}	1.05×10^{-2}	4.58×10^{0}	3.86×10^{-1}	-1.73×10^{-2}
	2(d)	0	8.14×10^{-1}	5.25×10^{-2}	0	-5.25×10^{-2}	-3.59×10^{-1}
	2(e)	-8.58×10^{-4}	-1.71×10^{-2}	-3.71×10^{-3}	-8.58×10^{-4}	3.71×10^{-3}	1.84×10^{-3}
	2(f)	4.14×10^{-1}	-6.20×10^{-1}	-3.81×10^{-2}	5.47×10^{-2}	-7.95×10^{-2}	2.55×10^{-3}

1. Crossed Box Graphs

The labeling of the momenta is shown in Fig. 5, where

$$p_1 = (E + p_0, \vec{p}),$$

$$p_3 = (p_0 - q_0, \vec{p} - \vec{q}),$$

$$p_2 = (E - q_0, -\vec{q}),$$

$$p_4 = (0, \vec{0}).$$

Renormalization is not required, and in order to obtain the result in terms of a Feynman integral we apply the Chisholm algebra.[14] We finally have

$$G(p,q) = (3 + 2\vec{\tau}_1\cdot\vec{\tau}_2)\left(\frac{g^2}{4\pi}\right)^2 \frac{1}{4\pi}\int dx_1 dx_2 dx_3 dx_4 \left\{[m-\gamma^{(1)}\cdot P^{(1)}][m-\gamma^{(2)}\cdot P^{(2)}]\frac{1}{\Delta^2} + \tfrac{1}{2}\gamma_\mu^{(1)}\gamma^{\mu(2)}\frac{1}{\Delta}\right\},$$

$$x_1 + x_2 + x_3 + x_4 = 1. \quad \text{(A1)}$$

Here the four-vectors $P^{(k)}$ are given by

$$P^{(k)} = p_k - \sum_{i=1}^{4} x_i p_i,$$

and (A2)

$$\Delta = \sum_{i=1}^{4} x_i(p_i^2 - \sigma_i) - \sum_{i,j=1}^{4} x_i x_j p_i p_j,$$

where σ_i means the squared mass of particle i.

2. Nucleon Self-Mass

We choose the labeling of the momenta as shown in Fig. 6(a). The nucleon self-mass results in the following replacement for the nucleon propagator:

$$\frac{i}{\not p - m} \to \frac{i}{\not p - m} + \frac{i}{\not p - m}[-i\Sigma(p)]\frac{i}{\not p - m},$$

with

TABLE II. Numerical results for the Feynman graphs of Fig. 2 for the $^3P_0$ partial wave at 50 and 200 MeV. The matrices are symmetric and we therefore have to present only six elements. We have put $g^2/4\pi = 1$.

	Fig.	(1, 1)	(1, 2)	(1, 3)	(2, 2)	(2, 3)	(3, 3)
50 MeV	2(a)	2.57×10^{-2}	-8.04×10^{-1}	2.23×10^{-1}	2.57×10^{-2}	-2.23×10^{-1}	2.71×10^{0}
	2(b)	1.16×10^{-3}	-1.64×10^{-2}	8.43×10^{-3}	3.05×10^{-1}	-1.79×10^{-1}	6.89×10^{-2}
	2(c)	-7.65×10^{-4}	-2.66×10^{-3}	-3.03×10^{-2}	3.51×10^{-1}	-1.45×10^{-1}	-4.67×10^{-1}
	2(d)	0	2.60×10^{-1}	-3.81×10^{-2}	0	3.81×10^{-2}	-9.20×10^{-1}
	2(e)	1.14×10^{-4}	-1.29×10^{-4}	9.84×10^{-4}	1.14×10^{-4}	-9.84×10^{-4}	8.54×10^{-3}
	2(f)	-5.47×10^{-5}	-2.05×10^{-1}	2.92×10^{-2}	-2.02×10^{-2}	5.78×10^{-2}	7.25×10^{-1}
200 MeV	2(a)	6.57×10^{-2}	-1.14×10^{0}	2.84×10^{-1}	6.57×10^{-2}	-2.84×10^{-1}	2.31×10^{0}
	2(b)	4.06×10^{-3}	-2.34×10^{-2}	1.42×10^{-2}	1.09×10^{-1}	-1.65×10^{-1}	4.75×10^{-2}
	2(c)	-6.18×10^{-3}	-5.73×10^{-3}	-8.92×10^{-2}	1.12×10^{0}	-3.07×10^{-1}	-7.67×10^{-1}
	2(d)	0	3.59×10^{-1}	-5.25×10^{-2}	0	5.25×10^{-2}	-8.14×10^{-1}
	2(e)	8.58×10^{-4}	-9.80×10^{-4}	3.71×10^{-3}	8.58×10^{-4}	-3.71×10^{-3}	1.62×10^{-2}
	2(f)	-4.14×10^{-4}	-2.83×10^{-1}	3.81×10^{-2}	-5.47×10^{-2}	7.95×10^{-2}	6.48×10^{-1}

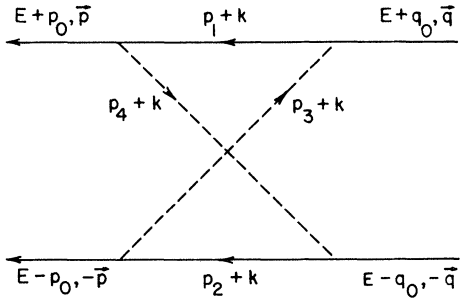

FIG. 5. Labeling of the external and internal momenta for the crossed box graph.

$$-i\Sigma(p)=3g^2\int\frac{d^4k}{(2\pi)^4}\frac{i}{k^2-\mu^2}\gamma_5\frac{i}{\not p-\not k-m}\gamma_5\,, \quad \text{(A3)}$$

3 being the isospin factor. The integral in (A3) is linearly divergent and two subtractions have to be performed:

$$-i\Sigma(p)=A+(\not p-m)B+(\not p-m)^2[-i\Sigma_f(p)]\,,$$

where A and B are infinite constants and Σ_f stands for the finite part. Introducing

$$\rho=\frac{p^2-\mu^2}{m^2}$$

and

$$\lambda=\frac{\mu}{m}\,,$$

we finally have

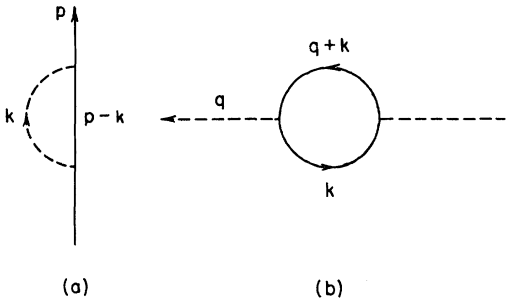

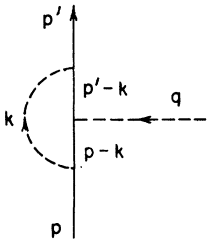

(c)

FIG. 6. Labeling of the momenta for (a) nucleon self-mass, (b) pion self-mass, (c) vertex correction.

$$\Sigma_f(p)=\Sigma_0(p)+(\not p+m)\Sigma_1(p)\,,$$

where

$$\Sigma_0(p)=\frac{g^2}{4\pi}\frac{3}{4\pi}\frac{1}{\rho m}S_0\,,$$

$$\Sigma_1(p)=\frac{g^2}{4\pi}\frac{3}{4\pi}\frac{1}{\rho m^2}S_1\,,$$

and

$$S_0=-\int_0^1 dx\,x\ln\left(1-\frac{\rho x(1-x)}{x^2+\lambda^2(1-x)}\right),$$

$$S_1=\int_0^1 dx(1-x)\ln\left(1-\frac{\rho x(1-x)}{x^2+\lambda^2(1-x)}\right)-2\int_0^1 dx\frac{x^2(1-x)}{x^2+\lambda^2(1-x)}\left[1+\frac{x^2+\lambda^2(1-x)}{\rho x(1-x)}\ln\left(1-\frac{\rho x(1-x)}{x^2+\lambda^2(1-x)}\right)\right].$$

These integrals can be performed analytically, and below the one-pion threshold $[\mathrm{Re}(\rho)<\lambda^2+2\lambda]$ we have

$$S_0=\frac{1-\lambda^2}{2(1+\rho)}-\frac{\ln\lambda^2}{4(1+\rho)}\left[1+2\lambda^2-\lambda^4-\frac{(1-\lambda^2)^2}{1+\rho}\right]$$

$$+\frac{1}{\rho}\left\{\frac{\lambda^2+\rho}{4(1+\rho)^2}[(\lambda^2-\rho)^2-4\lambda^2]^{1/2}\ln\frac{\lambda^2-\rho+[(\lambda^2-\rho)^2-4\lambda^2]^{1/2}}{\lambda^2-\rho-[(\lambda^2-\rho)^2-4\lambda^2]^{1/2}}+\tfrac{1}{2}\lambda^2(4\lambda^2-\lambda^4)^{1/2}\arccos\tfrac{1}{2}\lambda\right\}, \quad \text{(A4)}$$

$$S_1=\frac{3\lambda^2-1}{2(1+\rho)}+\frac{\ln\lambda^2}{4(1+\rho)}\left[1+4\lambda^2-3\lambda^4-\frac{(1-\lambda^2)^2}{1+\rho}\right]$$

$$+\frac{1}{\rho}\left\{\frac{\lambda^2}{1+\rho}-\frac{\rho^2-(\rho+2)\lambda^2}{4\rho(1+\rho)^2}[(\lambda^2-\rho)^2-4\lambda^2]^{1/2}\ln\frac{\lambda^2-\rho+[(\lambda^2-\rho)^2-4\lambda^2]^{1/2}}{\lambda^2-\rho-[(\lambda^2-\rho)^2-4\lambda^2]^{1/2}}\right.$$

$$\left.-\left[\left(\frac{5}{4}-\frac{1}{\rho}\right)(4\lambda^2-\lambda^4)-\tfrac{1}{4}\lambda^4\right]\frac{\lambda^2}{(4\lambda^2-\lambda^4)^{1/2}}\arccos\tfrac{1}{2}\lambda\right\}. \quad \text{(A5)}$$

3. Pion Self-Mass

The labeling of the momenta is shown in Fig. 6(b). The pion self-mass results in the replacement

$$\frac{i}{q^2-\mu^2}\delta_{ij}\to\frac{i}{q^2-\mu^2}\delta_{ij}+\frac{i}{q^2-\mu^2}K_{ij}\frac{i}{q^2-\mu^2}$$

for the pion propagator, with

$$K_{ij}=2\delta_{ij}K(q^2),$$

i and j being isospin indices, and

$$K(q^2)=-g^2\int\frac{d^4k}{(2\pi)^4}\frac{\mathrm{Tr}[(\not q+\not k+m)\gamma_5(\not k+m)\gamma_5]}{[(q+k)^2-m^2][k^2-m^2]}. \tag{A6}$$

The integral in (A6) is quadratically divergent and two subtractions have to be made:

$$K(q^2)=A+(q^2-\mu^2)B+(q^2-\mu^2)^2K_f(q^2),$$

where A and B are again infinite constants and K_f stands for the finite part. We finally obtain

$$\frac{1}{q^2-\mu^2}\to\frac{1}{q^2-\mu^2}+\frac{g^2}{4\pi}\frac{2}{\pi}I,$$

with

$$I=\int_0^1\frac{1}{q^2-\nu^2}\frac{x^2-\frac{1}{2}x}{1-x(1-x)\lambda^2}\times\left[\frac{1}{1-x}+\frac{x\lambda^2}{1-x(1-x)\lambda^2}\right]dx,$$

and

$$\nu^2=\frac{m^2}{x(1-x)}.$$

4. Vertex Correction

We choose the labeling of the momenta as shown in Fig. 6(c). The vertex correction results in the replacement

$$\gamma_5\to\gamma_5+\Lambda_5(p,p'),$$

with

$$\Lambda_5(p,p')=-(\vec\tau_1\cdot\vec\tau_2)g^2\int\frac{d^4k}{(2\pi)^4}\frac{i}{k^2-\mu^2}\gamma_5\frac{i}{\not p'-\not k-m}\times\gamma_5\frac{i}{\not p-\not k-m}\gamma_5. \tag{A7}$$

The integral in (A7) is logarithmically divergent and an infinite constant has to be subtracted:

$$\Lambda_5=L\gamma_5+\Lambda_{5f},$$

where

$$L=\Lambda_5(\not p=m,\not p'=m,q^2=\mu^2)$$

and Λ_{5f} is the finite part. We introduce

$$a^2=-m^2x^2+q^2y(x-y)+(p'^2-m^2)(1-x)(x-y)+(p^2-m^2)(1-x)y-\mu^2(1-x),$$

and

$$b^2=a^2(p^2=p'^2=m^2,q^2=\mu^2)=-m^2x^2+\mu^2[y(x-y)-(1-x)].$$

With

$$K_5=(1-x)(\not p'-m)\gamma_5(\not p-m)-mx[(\not p'-m)\gamma_5+\gamma_5(\not p-m)],$$

we finally have

$$\Lambda_{5f}=-(\vec\tau_1\cdot\vec\tau_2)\frac{g^2}{4\pi}\frac{1}{2\pi}\left\{\gamma_5\int_0^1dx\int_0^x dy\left[\ln\frac{a^2}{b^2}+\frac{\mu^2(1-x)}{2}\left(\frac{1}{a^2}-\frac{1}{b^2}\right)\right]+\frac{1}{2}\int_0^1dx\int_0^x dy\frac{K_5}{a^2}\right\}.$$

K_5 has been determined to vanish between positive-energy spinors but it contributes when sandwiched between negative-energy spinors, i.e., it contributes to all but the (1, 1) element of the Bethe-Salpeter kernels for the $J=0$ partial waves.

A partial integration with respect to y in the first part simplifies the partial-wave projection considerably.

The Dirac algebra for the sandwiching of the various graphs has been extensively described in Refs. 6 and 8, and a REDUCE code is available.[6] Therefore we consider it unnecessary to list the kernels in all details.

*Work performed under the auspices of the U. S. Atomic Energy Commission.

[1]P. Cziffra, M. H. MacGregor, M. J. Moravcsik, and H. P. Stapp, Phys. Rev. 114, 881 (1959); G. Breit, M. H. Hull, Jr., K. E. Lassila, and K. D. Pratt, Jr., *ibid.* 120, 2227 (1960); R. A. Bryan, Nucl. Phys. A146, 359 (1970).

[2]W. R. Wortman, in *The Padé Approximant in Theoretical Physics*, edited by G. A. Baker, Jr. and J. L. Gammel (Academic, New York, 1970), p. 333.

[3]J. L. Basdevant, in *Padé Approximants*, Lectures delivered at a summer school held at the University

of Kent, 1972, edited by P. R. Graves-Morris (The Institute of Physics, London and Bristol, 1973).
[4]D. Bessis, G. Turchetti, and W. R. Wortman, Phys. Lett. 39B, 601 (1972).
[5]R. H. Barlow and M. C. Bergère, Nuovo Cimento 11A, 557 (1972).
[6]J. Fleischer, Journal of Computational Physics (to be published).
[7]A. C. Hearn, REDUCE 2 User's Manual, Stanford Artificial Intelligence Project Memo AIM-133, 1970 (unpublished).
[8]T. Murota, M.-T. Noda, and F. Tanaka, Progr. Theoret. Phys. (Kyoto) 46, 1456 (1971); J. J. Kubis, Phys. Rev. D 6, 547 (1972).
[9]J. L. Gammel and M. T. Menzel, Phys. Rev. D 7, 565 (1973).
[10]J. L. Gammel, M. T. Menzel, and W. R. Wortman, Phys. Rev. D 3, 2175 (1971).
[11]D. Bessis, in *Padé Approximants* (Ref. 3).
[12]Experimental data taken from M. H. MacGregor, R. A. Arndt, and R. M. Wright, Phys. Rev. 182, 1714 (1969).
[13]G. Schierholz, Nucl. Phys. B40, 335 (1972); G. Kramer, in *Springer Tracts in Modern Physics*, edited by G. Höhler (Springer, New York, 1970), Vol. 55, p. 152.
[14]J. S. R. Chisholm, Proc. Cambridge Phil. Soc. 48, 300 (1952).

PHYSICAL REVIEW D VOLUME 8, NUMBER 5 1 SEPTEMBER 1973

Comparison of the Parton and Generalized Vector-Dominance Analyses of Deep-Inelastic Electron-Nucleon Scattering

Jean Pestieau
Institut de Physique Théorique, Université de Louvain, Louvain-la-Neuve, Belgium*
Jesús Urías†
Centro de Investigación y de Estudios Avanzados del Instituto Politécnico Nacional,‡ Mexico 14, D.F.
(Received 5 February 1973)

It is shown that, while generalized vector dominance is strictly applicable in the diffractive limit ($\nu \to \infty$, any $Q^2 \geq 0$ such that $x \equiv Q^2/2M\nu \to 0$) of electron-nucleon scattering and the parton model is applicable in the scaling limit ($Q^2 \to \infty$, x fixed), these two models are identical for describing the deep diffractive limit ($Q^2 \to \infty, x \to 0$). This equivalence is then used to interpret the different contributions of vector hadronic states which couple to the photon. A new scaling variable $\tilde{x}$ comes out naturally from our analysis.

The generalized vector-dominance model[1] has been made consistent with the present experimental data[2] of electron-nucleon scattering in the deep-inelastic region and can appear as an alternative for the parton model,[3] where the incident electron scatters elastically and incoherently off the point-like constituents of the target nucleon (Fig. 1). In the vector-dominance model, the collision between a (real or virtual) photon and a nucleon proceeds in two steps: (i) the photon (q) transforms into a vector hadronic state V, and then (ii) V collides with the nucleon (P). The total (virtual) photoabsorption cross section, which is proportional to the imaginary part of the (virtual) forward Compton scattering amplitude, is represented in Fig. 2:

$$[\gamma(q) \to V] + N(P) \to [V' \to \gamma(q)] + N(P) .$$

Only the three low-lying vector-meson contributions, $V = \rho, \omega, \phi$, were taken into account in the earlier versions of the vector-dominance model. However, it is clear now that these earlier versions are unsatisfactory at the phenomenological level for at least three reasons: (i) their failure to explain the total photoabsorption cross-section data, (ii) their prediction $\sigma_L >> \sigma_T$ for deep-inelastic electroproduction which is contrary to the experimental data, and (iii) the big e^+e^- annihilation hadronic cross sections at c.m. energy higher than 1.3 GeV. The generalized vector dominance has been proposed precisely to overcome these difficulties. Here V or V' are interpreted as any hadronic vacuum fluctuation of the photon, and not only as the low-lying mesons ρ, ω, ϕ but also the higher-mass vector mesons such as ρ' ($m_{\rho'} \sim 1.6$ GeV) *and* the nonresonating vector hadronic-state contributions with $J^c = 1^-$, which are very possibly not negligible at all. But this is not enough to fix the present form of the generalized vector-dominance model. For that, we have to introduce the further assumption, which can only be justified in the case of *diffraction*, that, if the ingoing photon in Compton scattering is coupled to a given hadronic vector state V, then the outgoing photon has to be coupled to the *same* hadronic state V. Therefore we take $V = V'$ in Fig. 2. This is analogous to the assumption of parton models, that in the scaling region, only elastic photon-parton scattering contributes (Fig. 1).